Lasers in Manufacturing Conference 2021

Scaling the throughput of high-quality silicon laser micromachining using a 1-kW sub-picosecond laser

Daniel Holder[a,*], Rudolf Weber[a], Christoph Röcker[a], Gerhard Kunz[b], David Bruneel[c], Martin Delaigue[d], Thomas Graf[a], Marwan Abdou Ahmed[a]

[a]*Institut für Strahlwerkzeuge (IFSW), University of Stuttgart, Pfaffenwaldring 43, 70569 Stuttgart, Germany*
[b]*Robert Bosch GmbH, Robert Bosch Campus 1, 71272 Renningen, Germany*
[c]*Lasea, Liège Science Park, Rue Louis Plescia 31, 4102 Seraing, Belgium*
[d]*Amplitude Systemes, 11, Avenue de Canteranne, 33600 Pessac, France*

Abstract

Recently, laser processing of silicon with ultrafast lasers has gained widespread attention for manufacturing of optics for THz radiation, an emerging topic with applications in medical imaging, security and communication. Such THz-optics require high-quality surfaces with low roughness in order to provide high transmission and low scattering. In the past, the low average power of ultrafast lasers limited the achievable throughput in silicon laser micromachining.
In this work a processing strategy for high-quality high-throughput micromachining of silicon with a 1-kW sub-picosecond laser is presented, which takes benefit of pulse bursts, low fluences and high feed rates.
As a result, laser micromachining could be demonstrated as a suitable technology for manufacturing of smooth structures on silicon while maintaining a high throughput. Surfaces with an appropriate roughness of $S_a \leq 0.6$ µm were produced with a high material removal rate of 230 mm³/min and a machining depth of up to 313 µm.

Keywords: Ultrafast laser ablation; silicon micromachining; upscaling; pulse burst; high quality; high throughput

1. Introduction

Laser processing with ultrafast lasers is a significantly growing field which offers high flexibility for advanced materials processing (Sugioka and Cheng, 2014). Laser micromachining of silicon has gained widespread attention for applications such as mask-free fabrication of silicon solar cells (Engelhart et al., 2007), dry etching

* Corresponding author. Tel.: +49 711 685 69740; fax: +49 711 685 66842.
E-mail address: daniel.holder@ifsw.uni-stuttgart.de.

of micro-electro-mechanical systems (MEMS) (Gower, 2001) and manufacturing of optics for THz radiation (Minkevičius et al., 2017), (Kononenko et al., 2020). Most of these applications require high surface quality with a low roughness of S_a < 1 µm and the absence of surface defects, e.g. to achieve low scattering and hence high transmission in optics for THz radiation (Indrisiunas et al., 2019). In the past, the average laser power limited the achievable throughput of ultrafast laser processes. With the upscaling of ultrafast lasers to powers exceeding 1 kW (Röcker et al., 2019), high throughput has been made possible in many applications. Furthermore, the first demonstration of a 10 kW ultrafast laser by (Müller et al., 2020) promises further significant increase of the productivity of laser applications in the future.

Recently, we reported on high-quality high-throughput laser micromachining of silicon with a sub-ps laser with more than 1 kW of average power, which was the first demonstration of material processing with sub-ps laser pulses at this power level (Holder et al., 2021). In this paper, additional insights about the scaling of the throughput and the resulting surface structure are presented.

2. Methods

The principle of the home-built ultrafast laser used for the experiments is described in detail in (Röcker et al., 2019). The specifications are summarized in Table 1.

Table 1. Specifications of the ultrafast laser used for the experiments

Parameter	Symbol	Value
Wavelength	λ	1030 nm
Pulse duration	τ	< 600 fs
Beam quality factor	M^2	< 1.5
Maximum average output power	P_{out}	1110 W
Repetition rate	f_b	500 kHz
Number of pulses within the burst	*PBB*	5
Intraburst pulse distance	-	22.7 ns

The experiments were performed in a processing station (Lasea, LS 5-1) with a focusing optic (Scanlab, varioSCAN$_{de}$ 40i) mounted to a Galvanometer-Scanner (Scanlab, intelliSCAN$_{de}$ 30). The specifications of the materials processing system are summarized in Table 2.

Table 2. Processing parameters on the sample surface

Parameter	Symbol	Value
Transmission of the optics in the station	-	91%
Maximum average power on the sample	P	1010 W
Maximum burst energy on the sample	E_b	2020 µJ
Focal length	-	580 mm
Focal diameter	d_0	90 µm
Size of scanning field	-	300 x 300 mm²

Silicon wafers with a crystal orientation of <100>, a diameter of 100 mm and a thickness of 1000 µm were micromachined in ambient air on the polished side of the wafers. Squares of 5 x 5 mm² were scanned along parallel offset lines with the hatching distance d_h using the sky-writing mode of the Galvanometer-Scanner to

ensure a constant feed rate v_s, resulting in a constant offset d_b between the impact locations of the individual bursts even at the maximum feed rate of 24 m/s. The depth of the micromachined cavities was increased by multiple scans over the same squares and measured by means of a 3D-Laser Scanning Microscope (LSM). The measured cavity depth d_c was used to calculate the immanent material removal rate

$$\Delta V_t = \frac{d_b \cdot d_h \cdot d_c \cdot f_b}{n_s}, \tag{1}$$

where d_b and d_h correspond to the offset of the impact locations of the bursts on the surface in and perpendicular to the feed direction, respectively, f_b denotes the repetition rate and n_s equals the number of scans over the processed area. The material removal rate represents the ablated material volume per unit of time and is typically used to evaluate the throughput of a micromachining process, i.e. the productivity. The energy-specific ablation volume of the process is defined by the ratio of the ablated volume and the irradiated energy and is obtained by

$$\Delta V_E = \frac{\Delta V_t}{P}, \tag{2}$$

where P denotes the average laser power. The surface quality was evaluated by measurement of the surface roughness S_a and investigation with a scanning electron microscope (SEM).

3. Results

The influence of the peak fluence per pulse on the resulting surface roughness and energy-specific volume was investigated. The focal position was set on the sample surface, which corresponds to a beam diameter on the surface of d_0 = 90 µm. A burst overlap of 78% on the surface in both directions was obtained with the feed rate of v_s = 10 m/s and the hatching distance d_h = 20 µm. The surface roughness (red triangles and left ordinate) and energy-specific volume (blue diamonds and right ordinate) as a function of the peak fluence per pulse by processing with n_s = 20 is shown in Fig. 1.

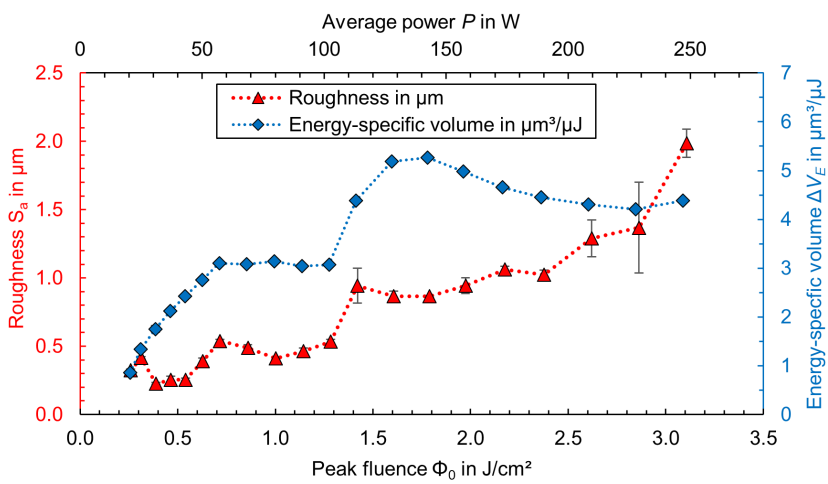

Fig. 1. Roughness S_a (red triangles and left ordinate) and energy-specific volume ΔV_E (blue diamonds and right ordinate) as a function of the peak fluence. Error bars represent the minimum and maximum deviation from three measurements. Process parameters: λ = 1030 nm, f_b = 500 kHz, PPB = 5, d_0 = 90 µm, v_s = 10 m/s, d_h = 20 µm, n_s = 20.

A low surface roughness $S_a < 0.6$ µm was achieved with peak fluences up to $\Phi_0 = 1.28$ J/cm², which corresponds to an average power of up to $P = 102$ W. The energy-specific volume increased with increasing peak fluence up to $\Delta V_E = 3.1$ µm³/µJ at $\Phi_0 = 0.72$ J/cm² and remained in this range up to $\Phi_0 = 1.28$ J/cm². The corresponding SEM images of micromachined surfaces with different peak fluences are shown in Fig. 2 a) and b). A low peak fluence of $\Phi_0 = 0.26$ J/cm² caused the formation of ripples with a spatial period in the range of the laser wavelength of 1 µm and formation of microgrooves (Fig. 2 a)). Nanoparticles are generated on the surface and the ripples appear blurry with a moderate peak fluence of $\Phi_0 = 0.72$ J/cm² (Fig. 2 b)). In the range of the optimum fluence from $\Phi_0 = 1.42$ J/cm² to $\Phi_0 = 2.38$ J/cm², which corresponds to an average power from $P = 113$ W to $P = 189$ W, the surface roughness remained in the range of $S_a \approx 1$ µm and a maximum energy-specific volume of $\Delta V_E = 5.3$ µm³/µJ was achieved. However, the peak fluences in this range caused the formation micrometer-sized solidified melt droplets and initiation of nanoscaled solidification cracks, also known as nanocracks (Fig. 2 c)). Further increase of the peak fluence and average power up to $\Phi_0 = 3.11$ J/cm² and $P = 247$ W, respectively, significantly increased the surface roughness to $S_a = 2.0$ µm. The nanocracks further propagated and were interconnected when the peak fluence of $\Phi_0 = 2.86$ J/cm² was applied (Fig. 2 d).

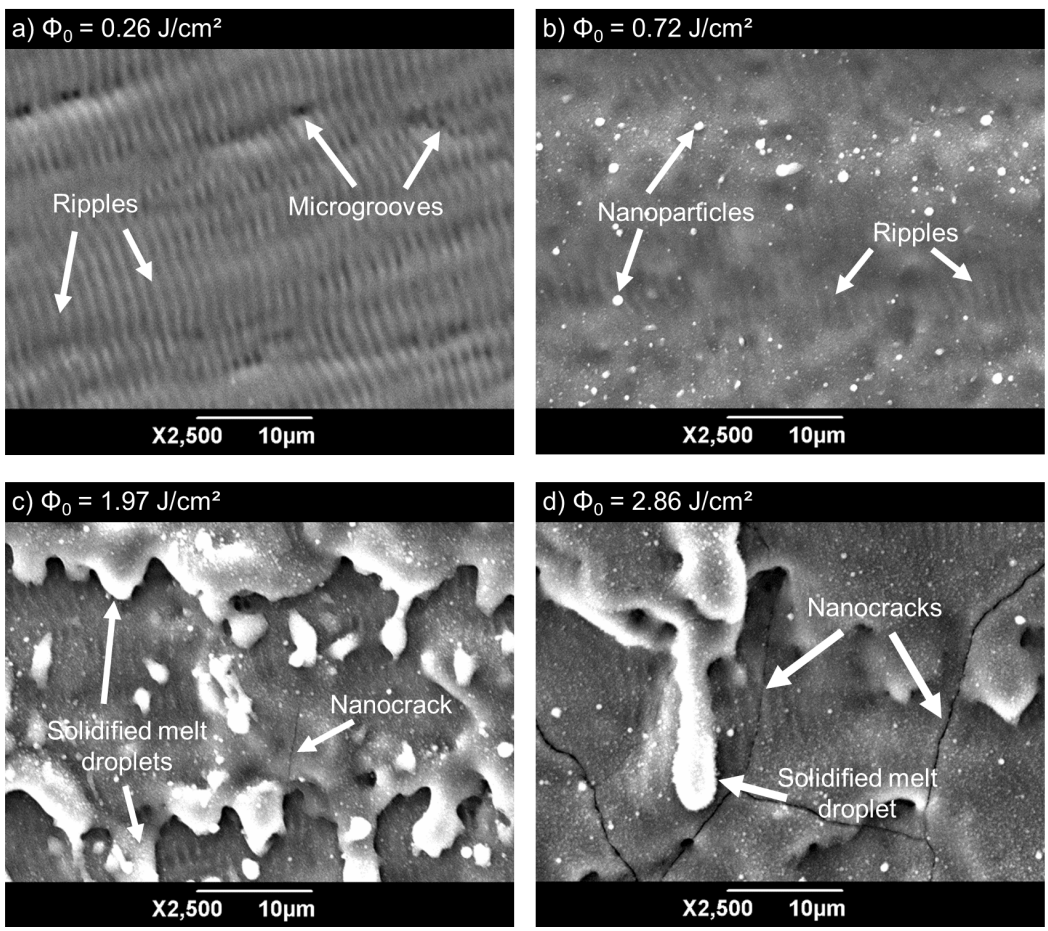

Fig. 2. SEM images of laser micromachined surfaces processed with different peak fluences a) $\Phi_0 = 0.26$ J/cm², b) $\Phi_0 = 0.72$ J/cm², c) $\Phi_0 = 1.97$ J/cm², and d) $\Phi_0 = 2.86$ J/cm². Process parameters: $\lambda = 1030$ nm, $f_b = 500$ kHz, PPB = 5, $d_0 = 90$ µm, $v_s = 10$ m/s, $d_h = 20$ µm, $n_s = 20$.

It can be seen from these results that high surface quality with a low roughness and avoidance of nanocracks while maintaining a sufficient energy-specific ablation volume can be achieved when a peak fluence in the range of Φ_0 = 0.72 J/cm² is used. The material removal rate at Φ_0 = 0.72 J/cm² and P = 57 W was calculated to ΔV_t = 10.6 mm³/min. For an increased throughput, the average laser power was increased from P = 57 W to P = 950 W, which led to an increase of the burst energy from E_b = 114 µJ to E_b = 1900 µJ. In order to maintain a moderate peak fluence of Φ_0 = 0.70 J/cm² at the burst energy of E_b = 1900 µJ, the beam diameter on the sample surface was increased from d_0 = 90 µm to d_0 = 372 µm by shifting the focus position of the laser beam 17 mm, which corresponds to approximately 4 Rayleigh lengths, below the sample surface. The increased amount of heat at this increased average power requires an adapted feed rate. The influence of the feed rate on the resulting surface roughness (red triangles and left ordinate) and energy-specific volume (blue diamonds and right ordinate) for laser micromachining of silicon at the high average power of P = 950 W is shown in Fig. 3. The number of scans n_s were adapted with respect to the feed rate v_s so that the incident number of pulses and hence the total incident laser energy per unit area remains at a constant value of 19 J/mm² for all investigated feed rates.

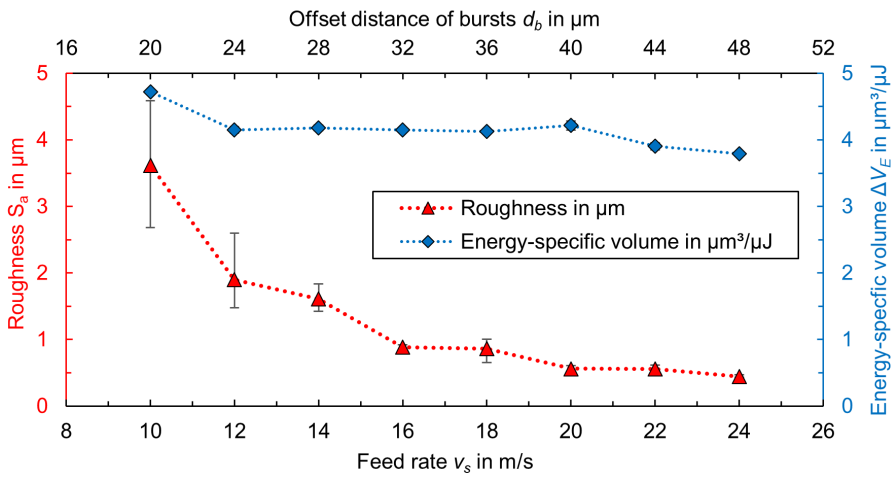

Fig. 3. Roughness S_a (red triangles and left ordinate) and energy-specific volume ΔV_E (blue diamonds and right ordinate) of the micromachined surfaces as a function of the feed rate with adapted number of scans to keep to total incident energy per unit area at a constant value of 19 J/mm². Error bars represent the minimum and maximum deviation from three measurements. Process parameters: λ = 1030 nm, P = 950 W, f_b = 500 kHz, Ep = 1900 µJ, PPB = 5, d_0 = 372 µm, Φ_0 = 0.70 J/cm², d_h = 50 µm.

With the increased beam diameter of d_0 = 372 µm which was chosen to keep the peak fluence at the desired value of Φ_0 = 0.70 J/cm², the roughness obtained at a feed rate of v_s = 10 m/s and a spatial offset distance of bursts of d_b = 20 µm amounts to S_a = 3.6 µm which is significantly higher than the one obtained in the experiments with P = 57 W. At this low feed rate, the elevated surface temperature caused by the high average power P = 950 W led to the formation of melt and nanocracks (Fig. 4 a). With increasing feed rate and thus increasing offset distance of bursts, the roughness decreases up to the lowest achieved value of S_a = 0.4 µm at the maximum feed rate of v_s = 24 m/s, the latter corresponding to a spatial offset distance of bursts of d_b = 48 µm. The surface obtained with v_s = 24 m/s is shown in Fig. 4 d). It is covered with ripples and nanoparticles without larger surface damage. A major transition of the surface quality occurs in the feed rate range of 14 m/s to 16 m/s, also referred to as the critical feed rate (Bauer et al., 2015). At v_s = 14 m/s and below, a roughness S_a > 1 µm was measured and the surface was mainly characterized by solidified melt films and nanocracks (Fig. 4 a) and b)), with wider cracks appearing at lower feed rates. At v_s = 16 m/s and above,

the roughness was S_a < 1 µm and the surface was covered only with ripples and nanoparticles (Fig. 4 c) and d)). The energy-specific volume also decreased from ΔV_E = 4.7 µm³/µJ at v_s = 10 m/s to ΔV_E = 3.8 µm³/µJ at v_s = 24 m/s. Interestingly, the energy-specific volume remained constant in the range of the critical feed rate, where a major transition of the surface quality occurred. The comparison of the results achieved at high power (P = 950 W) and v_s = 24 m/s (cf. Fig. 4 d)) with the results achieved at low power (P = 57 W) and v_s = 10 m/s (cf. Fig. 2 b)) shows similar surface structures and roughness values with S_a = 0.4 µm and S_a = 0.5 µm, respectively. However, at a power P = 950 W, the material removal rate is increased by a factor of 20 from ΔV_t = 10.6 mm³/min to ΔV_t = 216.0 mm³/min.

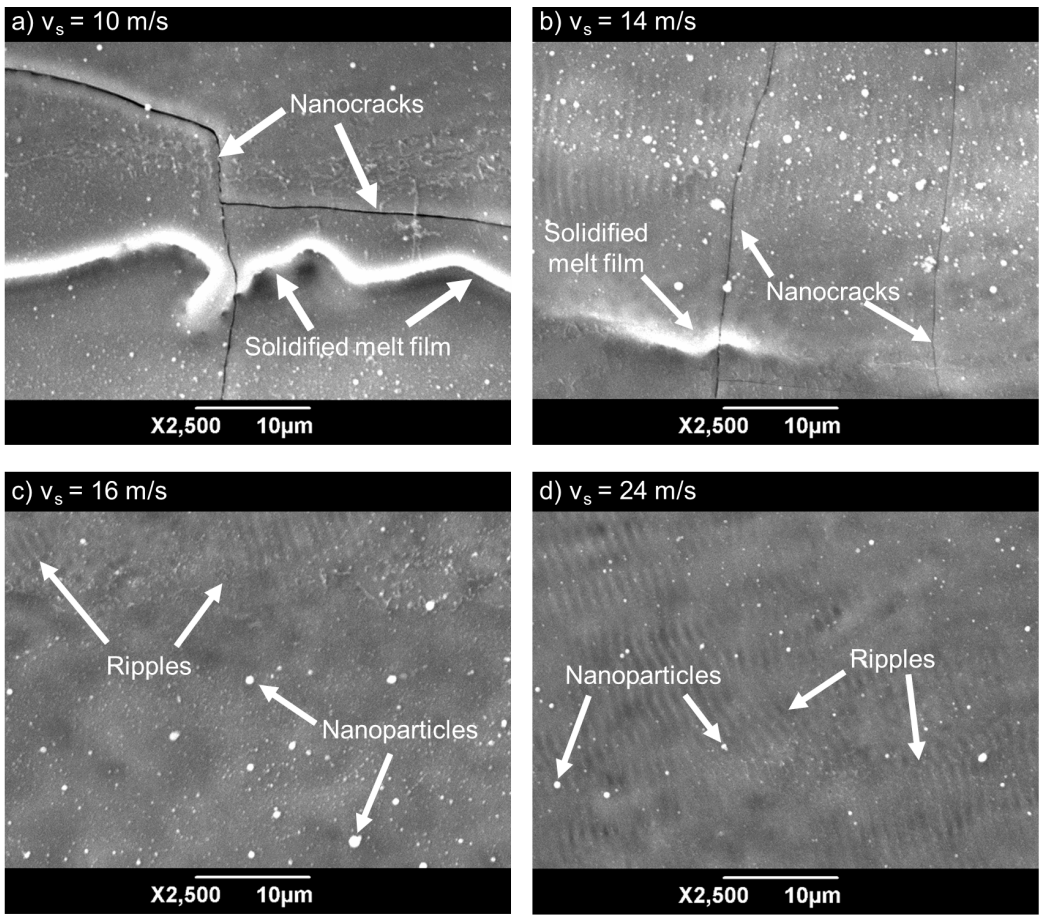

Fig. 4. SEM images of laser micromachined surfaces processed with different feed rates and adapted number of scans to keep to total incident energy per unit area at a constant value of 19 J/mm². a) v_s = 24 m/s, b) v_s = 16 m/s, c) v_s = 14 m/s, and d) v_s = 10 m/s. Process parameters: λ = 1030 nm, P = 950 W, f_b = 500 kHz, Ep = 1900 µJ, PPB = 5, d_0 = 372 µm, Φ_0 = 0.70 J/cm², d_h = 50 µm.

The cavity depth of micromachined surfaces with v_s = 24 m/s and n_s = 20 was measured to d_c = 72 µm. A high surface quality with a low roughness and avoidance of nanocracks or other surface defects have to be maintained over a range of the cavity depth from a few microns up to several hundreds of microns in order to ensure surfaces that are suitable for the manufacturing of demanding devices such as THz optics. The cavity depth can be adjusted by adaption of the number of scans over the processed area. The surface roughness

(red triangles and left ordinate) and cavity depth (green squares and right ordinate) of the micromachined surfaces after processing with P = 950 W, Φ_0 = 0.70 J/cm² and v_s = 24 m/s for various number of scans up to 100 are shown in Fig. 5 a).

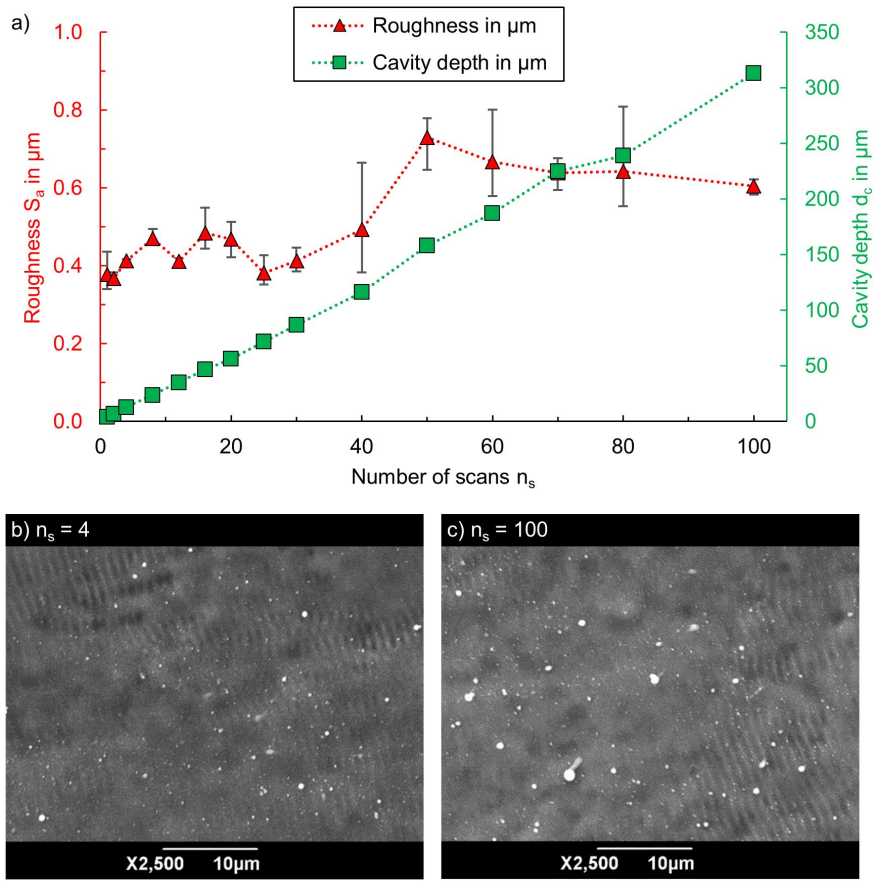

Fig. 5. a) Roughness (red triangles and left ordinate) and cavity depth (green squares and right ordinate) of the micromachined surfaces as a function of the number of scans. SEM images corresponding surfaces at b) n_s = 4 and c) n_s = 100. Process parameters: λ = 1030 nm, P = 950 W, f_b = 500 kHz, Ep = 1900 µJ, PPB = 5, Φ_0 = 0.70 J/cm², d_0 = 372 µm, v_s = 24 m/s, d_h = 50 µm.

Two distinct regimes can be identified with respect to the resulting surface roughness S_a. The first regime with a roughness S_a < 0.5 µm reaches until a maximum of about 40 scans, which corresponds to a cavity depth of d_c = 116 µm. The micromachined depth per scan in this first regime is approximately 3.0 µm. The second regime exhibits an increased roughness of 0.6 µm < S_a < 0.8 µm and ranges from 50 to 100 scans up to the maximum investigated cavity depth of d_c = 313 µm. The micromachined depth per scan in the second regime is approximately 3.2 µm. In the present work, a low roughness S_a < 0.8 µm and fine surface structure partially covered with ripples and nanoparticles could be maintained up to the maximum milled depth of 313 µm (Fig. 5 b) and c)). Both are required to avoid scattering and achieve maximum transmission when laser micromachining is used for the manufacturing of optics for THz radiation.

Finally, laser micromachining of a chamfer geometry and the logo of the institute on the surface of a silicon wafer was demonstrated with 1.01 kW average laser power on the sample surface. With a constant beam diameter of d_0 = 372 µm the resulting peak fluence was slightly increased to Φ_0 = 0.74 J/cm². The chamfer geometry of the size 5 x 5 mm² shown in Fig. 6 a) was micromachined by decreasing the width of one side of the scanning area after each scan by 50 µm, which corresponds to one parallel offset line. The logo of the institute with a size of 80 x 25 mm² was micromachined on the silicon wafer using n_s = 10 scans and is shown in Fig. 6 b).

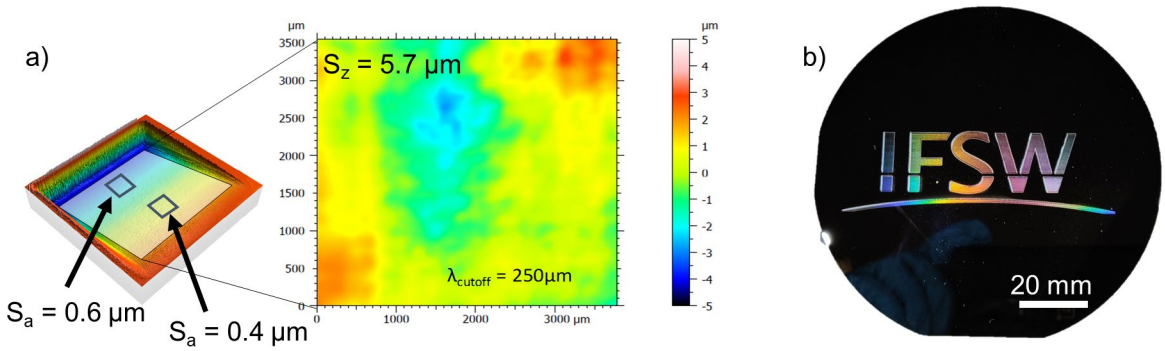

Fig. 6. a) LSM measurement of a chamfer and b) photograph of the logo of the institute micromachined on the surface of a silicon wafer and illuminated by white light. Process parameters: λ = 1030 nm, P = 1010 W, f_b = 500 kHz, Ep = 2020 µJ, PPB = 5, Φ_0 = 0.74 J/cm², d_0 = 372 µm, v_s = 24 m/s, d_h = 50 µm.

The LSM measurements revealed low roughness values, with S_a = 0.4 µm in the upper area of the chamfer geometry and S_a = 0.6 µm in the lower area of the chamfer geometry (Fig. 6 a)). The surface was again covered with ripples and nanoparticles (not shown here). This is consistent with the results obtained for laser micromachining of the flat surfaces shown in Fig. 5. Furthermore, the flatness of the tilted surface was investigated by calculation of the peak-to-valley height after filtering the LSM measurement with a cutoff wavelength of 250 µm. The tilted surface is smooth with a low peak-to-valley height of 5.7 µm over the large area of 3.5 x 3.5 mm². Although the micromachined depth per scan was about 3 µm, no steps were detected along the offset parallel processed lines. The illumination of the micromachined wafer shown in Fig. 6 b) with white light caused the appearance of varying colors at different view angles, due to the diffractive behavior of the grating-like ripples. The results demonstrate the capability of high-quality micromachining with high average power over a large area when an appropriate processing strategy is used. The energy-specific volume of ΔV_E = 3.8 µm³/µJ during laser micromachining with P = 1010 W corresponds to a high material removal rate of ΔV_t = 230 mm³/min. To the best of our knowledge, this is the highest material removal rate reported so far for laser micromachining of silicon with ultrafast lasers, while at the same time achieving high surface quality with $S_a \leq$ 0.6 µm and no surface defects with diameters exceeding 1 µm.

4. Conclusion

In summary, high-quality high-throughput silicon laser micromachining with an ultrafast laser delivering an average power of >1 kW is presented. A low surface roughness $S_a \leq$ 0.6 µm and smooth surface structure with ripples and nanoparticles was obtained at high average power by using pulse bursts, low peak fluences, and high feed rates. Furthermore, a low roughness was maintained up to the maximum investigated micromachining depth of 313 µm. The energy-specific volume was measured to be ΔV_E = 3.8 µm³/µJ at 1010 W

on the workpiece, which corresponds to a material removal rate of ΔV_t = 230 mm³/min. Hence, high-power ultrafast lasers in combination with appropriate processing strategies can significantly enhance the throughput while maintaining high surface quality.

Acknowledgements

This project has received funding from the European Union's Horizon 2020 Research and Innovation Program under Grant Agreement No 687880. The authors thank Liane Hoster and Johannes Wahl for their support with the SEM images and Gennadij Nikitin for his support with LSM measurements.

References

Bauer, F., Michalowski, A., Kiedrowski, T., Nolte, S., 2015. Heat accumulation in ultra-short pulsed scanning laser ablation of metals. Optics express 23 (2), 1035–1043. doi:10.1364/OE.23.001035.

Engelhart, P., Harder, N.-P., Grischke, R., Merkle, A., Meyer, R., Brendel, R., 2007. Laser structuring for back junction silicon solar cells. Prog. Photovolt: Res. Appl. 15 (3), 237–243. doi:10.1002/pip.732.

Gower, M.C., 2001. Laser micromachining for manufacturing MEMS devices, in: MEMS Components and Applications for Industry, Automobiles, Aerospace, and Communication. Micromachining and Microfabrication, San Francisco, CA. Monday 22 October 2001. SPIE, pp. 53–59.

Holder, D., Weber, R., Röcker, C., Kunz, G., Bruneel, D., Delaigue, M., Graf, T., Ahmed, M.A., 2021. High-quality high-throughput silicon laser milling using a 1 kW sub-picosecond laser. Optics letters 46 (2), 384–387. doi:10.1364/OL.411412.

Indrisiunas, S., Svirplys, E., Richter, H., Urbanowicz, A., Raciukaitis, G., Hagelschuer, T., Hubers, H.-W., Kasalynas, I., 2019. Laser-Ablated Silicon in the Frequency Range From 0.1 to 4.7 THz. IEEE Trans. THz Sci. Technol. 9 (6), 581–586. doi:10.1109/TTHZ.2019.2939554.

Kononenko, T.V., Knyazev, B.A., Sovyk, D.N., Pavelyev, V.S., Komlenok, M.S., Komandin, G.A., Konov, V.I., 2020. Silicon kinoform cylindrical lens with low surface roughness for high-power terahertz radiation. Optics & Laser Technology 123, 105953. doi:10.1016/j.optlastec.2019.105953.

Minkevičius, L., Indrišiūnas, S., Šniaukas, R., Voisiat, B., Janonis, V., Tamošiūnas, V., Kašalynas, I., Račiukaitis, G., Valušis, G., 2017. Terahertz multilevel phase Fresnel lenses fabricated by laser patterning of silicon. Optics letters 42 (10), 1875–1878. doi:10.1364/OL.42.001875.

Müller, M., Aleshire, C., Klenke, A., Haddad, E., Légaré, F., Tünnermann, A., Limpert, J., 2020. 10.4 kW coherently combined ultrafast fiber laser. Optics letters 45 (11), 3083–3086. doi:10.1364/OL.392843.

Röcker, C., Loescher, A., Delaigue, M., Hönninger, C., Mottay, E., Graf, T., Abdou Ahmed, M., 2019. Flexible Sub1- ps Ultrafast Laser Exceeding 1 kW of Output Power for High-Throughput Surface Structuring. OSA Laser Congress 2019 (ASSL, LAC, LS&C), 1–2.

Sugioka, K., Cheng, Y., 2014. Ultrafast lasers—reliable tools for advanced materials processing. Light Sci Appl 3 (4), 1-12. doi:10.1038/lsa.2014.30.